



**HAL**  
open science

## Assessment of kinetic models for the production of $\gamma$ -valerolactone developed in isothermal, adiabatic and isoperibolic conditions

Wenel Naudy Vásquez Salcedo, Mélanie Mignot, Bruno Renou, Sébastien Leveneur

### ► To cite this version:

Wenel Naudy Vásquez Salcedo, Mélanie Mignot, Bruno Renou, Sébastien Leveneur. Assessment of kinetic models for the production of  $\gamma$ -valerolactone developed in isothermal, adiabatic and isoperibolic conditions. *Fuel*, 2023, 350, pp.128792. 10.1016/j.fuel.2023.128792 . hal-04115376

**HAL Id: hal-04115376**

**<https://normandie-univ.hal.science/hal-04115376v1>**

Submitted on 2 Jun 2023

**HAL** is a multi-disciplinary open access archive for the deposit and dissemination of scientific research documents, whether they are published or not. The documents may come from teaching and research institutions in France or abroad, or from public or private research centers.

L'archive ouverte pluridisciplinaire **HAL**, est destinée au dépôt et à la diffusion de documents scientifiques de niveau recherche, publiés ou non, émanant des établissements d'enseignement et de recherche français ou étrangers, des laboratoires publics ou privés.

1           **Assessment of kinetic models for the production of  $\gamma$ -valerolactone developed in**  
2                           **isothermal, adiabatic and isoperibolic conditions**

3           Wenel Naudy Vásquez Salcedo<sup>1,2</sup>, Mélanie Mignot<sup>3</sup>, Bruno Renou<sup>2</sup>, Sébastien Leveneur<sup>1\*</sup>

4           <sup>1</sup>*INSA Rouen Normandie, UNIROUEN, Normandie Univ, LSPC, UR4704, F-76000 Rouen,*  
5           *France, France, Corresponding author (\*): [sebastien.leveneur@insa-rouen.fr](mailto:sebastien.leveneur@insa-rouen.fr)*

6           <sup>2</sup>*Normandie Univ., UNIROUEN, INSA Rouen, CNRS, CORIA, 76000 Rouen, France*

7           <sup>3</sup>*Normandie Université, INSA Rouen, UNIROUEN, CNRS, COBRA Laboratory, F-76000 Rouen,*  
8           *France*

9

10

11 **Abstract**

12 The use of lignocellulosic biomass as raw materials for the production of biofuels is increasing. There  
13 are several potential processes valorizing these raw materials, but the shift from lab-scale to industrial  
14 scale requires the development of reliable and robust kinetic models. Usually, these models are  
15 developed in isothermal mode, limiting their use for thermal risk assessment or pinch analysis. We  
16 developed and assessed several kinetic models for the hydrogenation of butyl levulinate to  $\gamma$ -  
17 valerolactone over Ru/C in different thermal modes, i.e., isothermal, isoperibolic and adiabatic modes.  
18 The reaction calorimeter Mettler-Toledo RC1 was used to perform kinetic experiments. Bayesian  
19 inference was used during the regression stage to calculate the credible intervals. The validation stage  
20 was done by a holdout method. From the regression and validation stage, we found that the non-  
21 competitive Langmuir Hinshelwood with hydrogen non-dissociation and dissociation were the most  
22 reliable models. These models can predict the kinetics of this reaction system in different thermal modes.

23 **Keywords:** kinetic modeling, gamma valerolactone, levulinate, calorimetry, adiabatic

24

25 **Abbreviations**

$C_p$	Specific heat capacity [ $\text{J}\cdot\text{kg}^{-1}\cdot\text{K}^{-1}$ ]
$E_a$	Activation energy [ $\text{J}\cdot\text{mol}^{-1}$ ]
$f_{iu}(\xi)$	Estimated concentration or temperature
$H_e$	Henry's coefficient [ $\text{mol}\cdot\text{m}^{-3}\cdot\text{bar}^{-1}$ ]
$k$	Rate constant
$K_i$	Adsorption rate of specie $i$ [ $\text{m}^3\cdot\text{mol}^{-1}$ ]
$k_{L,a}$	Volumetric mass transfer coefficient [ $\text{s}^{-1}$ ]
$(k_{L,a})_{\text{modified}}$	Modified volumetric mass transfer coefficient [ $(\text{Pa}\cdot\text{s}\cdot\text{K}^{-1})^{0.5}(\text{Pa}\cdot\text{s}\cdot\text{kg}^{-1}\cdot\text{m}^{-3})^{0.25}\cdot\text{s}^{-1}$ ]
$m$	Mass [ $\text{kg}$ ]
$P$	Pressure [ $\text{bar}$ ]
$R_i$	Reaction rate $i$ [ $\text{mol}\cdot\text{m}^{-3}\cdot\text{s}^{-1}$ ]
$R$	Gas constant [ $\text{J}\cdot\text{mol}^{-1}\cdot\text{K}^{-1}$ ]
$T$	Temperature [ $\text{K}$ ]
$UA$	Global heat transfer coefficient [ $\text{W}\cdot\text{K}^{-1}$ ]
$ v(\xi) $	Determinant of the covariance matrix of responses
$Y_i$	Experimental concentration of specie $i$ or temperature

26

27 **Greek letters**

$\omega_{Cat.}$	Catalyst loading [ $\text{kg}\cdot\text{m}^{-3}$ ]
$\mu_{liq}$	Liquid viscosity [ $\text{Pa}\cdot\text{s}$ ]
$\rho_{liq}$	Mass density [ $\text{kg}\cdot\text{m}^{-3}$ ]

28

29

30

31

32 Subscripts and superscripts

Liq	Liquid phase
Ref	Reference
o	Initial
*	Interfacial value

33

34 Abbreviations

AIC	Akaike information criterion
BL	Butyl levulinate
BHP	Butyl 4-hydroxypentanoate
BuOH	Butanol
ER	Eley-Rideal kinetic model with no adsorption of hydrogen
GC	Gas chromatography
GVL	$\gamma$ -valerolactone
HPD	Highest Posterior Density
LH1	Langmuir-Hinshelwood kinetic model with molecular adsorption of hydrogen
LH2	Langmuir-Hinshelwood kinetic model with hydrogen dissociation
NCLH1	Non-competitive Langmuir-Hinshelwood kinetic model with no dissociation of hydrogen
NCLH2	Non-competitive Langmuir-Hinshelwood kinetic model with hydrogen dissociation
ODEs	Ordinary differential equation system
OF( $\xi$ )	Objective function
RKMC	Redlich-Kwong-Mathias-Copeman equation of state
Ru/C	Ruthenium on activated carbon

35

36 1. Introduction

37 Our dependency on fossil raw materials is very high in the modern society. Over 80% of the world's  
38 primary energy consumption in the energy sector was from fossil raw materials in 2020 [1].

39 The use of lignocellulosic biomass (LCB) for biofuel production is seen as a better alternative to fossil  
40 fuel because of its global availability, lower environmental impact, and cost [2–6]. Besides, such raw  
41 materials are not in competition with the alimentary sector, avoiding the dilemma of food versus fuel  
42 [7,8]. The sugar parts of LCB, i.e., cellulose and hemicellulose, are mainly used to produce chemicals,  
43 materials or fuels. The valorization of these polymers of sugar can lead to several platform molecules  
44 and their derivatives, such as succinic acid, furfural, 5-HMF, levulinic acid, glycerol, etc. [9–12].

45 The chemical  $\gamma$ -valerolactone (GVL), produced from the hydrogenation of levulinic acid or ester  
46 levulinate, is also considered as a platform molecule [13,14]. Hydrogenation of bio-based carboxylic  
47 acids, esters or related compounds is considered a step toward a sustainable and carbon-neutral process  
48 [15]. In fine chemistry, GVL is considered an excellent aprotic solvent [16–21] because of its low vapor  
49 pressure, high flash point, and potential to increase acid activity [22–26]. In polymer science, GVL is a  
50 promising starting material for producing greener monomers [27–30].

51 In the energy field, GVL cannot be used directly as a fuel [31], but it can be used as an additive fuel  
52 [32–35]. GVL is a promising feedstock for producing hydrocarbon fuels [31,36–42] or pentanoic  
53 biofuels [43].

54 From a safety, cost and environmental standpoint, determining the best operating conditions for the  
55 production of GVL is vital [44–46]. The literature proposes several routes for producing GVL by  
56 hydrogenating raw lignocellulosic biomass, cellulose, glucose or fructose [47]. These different routes  
57 require the hydrogenation of levulinic acid or alkyl levulinates, and there are three different  
58 hydrogenation options:

59 -use of molecular hydrogen [34,48–65]

60 -*in situ* FA decomposition producing hydrogen [66–74]

61 -Meerwein-Ponndorf-Verley reaction involving the use of alcohol for hydrogen transfer [75–82]

62 The use of molecular hydrogen and ruthenium-based catalyst is the most efficient system to produce  
63 GVL. Developing such a process at an industrial scale requires reliable and robust kinetic models. Such  
64 models are essential to optimize the operating cost to get the highest GVL yield. There are several  
65 models for the hydrogenation of levulinates or levulinic acid [52,53,57,64,83–87]. These models were  
66 developed using experiments performed in isothermal mode, and could limit their application to pinch  
67 analysis or process safety.

68 Generally speaking, the development of kinetic models in different thermal modes, e.g., isothermal,  
69 adiabatic, isoperibolic, or dynamic modes, is quite seldom in the literature.

70 In adiabatic mode, one can only use the reaction temperature as an observable [88–90] allowing to obtain  
71 reliable models for thermal risk assessment [91]. It is impossible to withdraw samples during the  
72 reaction; otherwise, the reaction temperature signal is perturbed. Hence, kinetic models only developed  
73 in adiabatic mode are limited for thermal risk assessment.

74 In isoperibolic mode, for some chemical systems, it is possible to track the reaction temperature and  
75 withdraw some samples to track the concentration in the liquid phase [92–94], allowing the development  
76 of reliable kinetic models considering concentration and temperature as observables.

77 There is a need to have kinetic models developed in different thermal modes to improve their reliability  
78 and robustness and to be used universally for process safety, process intensification, and cost evaluation.  
79 To do that, one must carry out different experiments in isothermal conditions to track the species  
80 concentration and in non-isothermal conditions (isoperibolic and adiabatic modes) to track the reaction  
81 temperature.

82 To the best of the authors' knowledge, such an approach is highly seldom in the literature [94]. In this  
83 study, we developed kinetic models for the hydrogenation of butyl levulinate into GVL over Ru/C in  
84 three thermal modes: isothermal, isoperibolic and adiabatic. A high concentrated solution of BL was  
85 used to perform experiments. The state-of-the-art reaction calorimeter Mettler-Toledo RC1 was used to  
86 perform experiments in different thermal modes. The developed models were validated to assess their

87 reliability and select the most reliable ones. Butyl levulinate was chosen because it is gaining a lot of  
88 interest as a platform molecule and can be used in different areas [16,95].

89



90 2. Experimental section

91 2.1. Chemicals

92 Chemicals used during this research for analytical and experimental purposes were purchased from  
93 different providers and used without further purification: n-Butyl levulinate (n-BL), acquired from Alfa  
94 Aesar with a purity  $\geq 98\%$ , CAS: 2052-15-5. Hydrogen gas ( $H_2$ ), acquired from Linde group with a  
95 purity  $\geq 99.99\%$ , CAS: 1333-74-0.  $\gamma$ -Valerolactone (GVL), acquired from Sigma Aldrich with a purity  
96  $\geq 99\%$ , CAS: 108-29-2. 1-Butanol (BuOH), acquired from LabLine with a purity  $\geq 99\%$ , CAS: 71-36-  
97 3. Ruthenium on activated carbon (Ru/C), acquired from Alfa Aesar, 5% of ruthenium powder, reduced,  
98 50% nominally wet, CAS: 7440-18-8. Acetone, acquired from Fischer Scientific with a purity  $\geq 99\%$ ,  
99 CAS: 67-64-1.

100

101 2.2. Analytical system

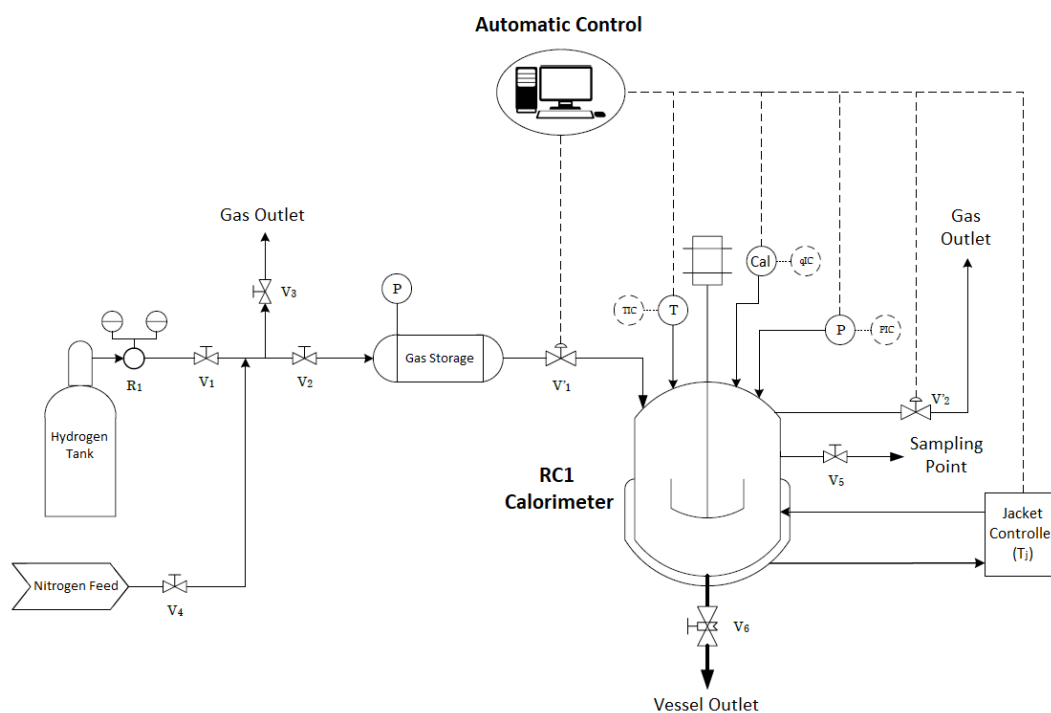
102 Gas chromatography coupled with a flame ionization detector (GC-FID) technique was applied to  
103 quantify the amount of chemicals in samples. GC-FID equipment is from Scion Instruments supplier.  
104 GC-FID was equipped with a low polarity column (Phenomenex, ZB-5) composed of 95% dimethyl  
105 siloxane and 5% of phenyl groups. Column dimensions: length: 30 m, internal diameter: 0.32 mm,  
106 coating width: 0.25  $\mu\text{m}$ .

107 Helium (99.99%) was used as carrier gas at a constant flow rate of 1.2 mL/min. The temperature of the  
108 injector and the detector were set at 250 °C. The oven temperature ramp was set to 50 °C (1 min) – 20  
109 °C /min – 200 °C (1 min). Samples were diluted in acetone to be analyzed, the injection volume was 1  
110  $\mu\text{L}$  and the split ratio was 20:1.

111 2.3. RC1 reactor

112 To develop a robust kinetic model for GVL production from n-BL, different experiments were  
113 performed in the Mettler-Toledo RC1mx calorimeter, considering isothermal and non-isothermal  
114 conditions.

115 The RC1mx is a high-performance calorimeter with a heating and cooling loop system, allowing us to  
116 have a very accurate temperature control of the reaction media. The RC1mx vessel is made of Hastelloy  
117 C22 metal one, with a 1.8 L capacity and 100 bar of tolerance. A gas inlet and outlet system are  
118 connected to the vessel to control the pressure. A PID automatically controls this system. The RC1mx  
119 is also equipped with a calibration heater that evaluates the heat capacity ( $C_p$ ) and the reaction media's  
120 global heat transfer coefficient ( $UA$ ). Fig. 1 represents the RC1mx installation.



121

122 Fig. 1. RC1mx Calorimeter installation.

123

124 2.4. Determination of the global heat transfer

125 The global heat transfer UA plays a fundamental role in the energy balance to characterize the transfer  
126 between the heat carrier and reaction temperature. Thus, it is vital to measure it correctly. This value  
127 was determined by electrical calibration [96–98]. Calibration experiments were performed without  
128 catalysts, and a highly concentrated solution of BL, i.e., weight percentage higher than 98%, was used  
129 initially. We varied the temperature and rotating speed to be able to draw the Wilson plot.

130 2.5. Gas-liquid mass transfer measurement

131 Table 1 shows the experimental matrix for mass transfer study. These experiments were performed in  
132 the absence of catalyst to avoid chemical reactions. The Redlich–Kwong–Mathias–Copeman (RKMC)  
133 equation of state was used to quantify the number of moles of hydrogen into the gas phase. According  
134 to Nasrifar, the RKMC equation is more accurate and robust [99].

135 Table 1. Experimental matrix for gas-liquid mass transfer measurement.

<b>Run</b>	<b>m<sub>0</sub>BL (kg)</b>	<b>Tr<sub>0</sub> (K)</b>	<b>P (bar)</b>
<b>1_MT</b>	0.520	373.15	25
<b>2_MT</b>	0.520	373.15	25
<b>3_MT</b>	0.520	413.15	25
<b>4_MT</b>	0.520	433.15	25

136

137

138

139 2.6. Kinetic modeling

140 Parameter estimation, simulation and curve fitting were performed using the commercial software  
141 Athena Visual Studio V.14.2 [100]. Athena Visual Studio uses a Bayesian framework more suitable for  
142 multi-response parameter estimation than the classical nonlinear least squares method [101,102].  
143 Indeed, Bayesian inference requires calculating the determinant criterion [103].

144 The following observables were used for the parameter estimation stage: BL, BHP, GVL and reaction  
145 temperatures. Only two samples were withdrawn for experiments performed in isoperibolic or adiabatic  
146 conditions: at the beginning and the end of the reaction. Several samples were withdrawn for isothermal  
147 kinetic experiments, and the reaction temperature was constant.

148 The ODEs, obtained from material and energy balances, were integrated by the DDAPLUS solver, a  
149 modified Newton algorithm [104]. The GREGPLUS subroutine package was used to minimize the  
150 objective function  $OF(\xi)$  and to calculate the highest probability density HPD, i.e., credible intervals, of  
151 the estimated parameters and the normalized covariance matrix.

152 GREGPLUS uses successive quadratic programming starting from our initial guess values to minimize  
153  $OF(\xi)$  [100].

$$154 \quad OF(\xi) = (a + b + 1) \cdot \ln|v(\xi)| \quad (1)$$

155 where  $a$  is the number of events in response,  $b$  is the number of responses and  $|v(\xi)|$  is the  
156 determinant of the covariance matrix of the responses.

157 Each element of the covariance matrix of the responses is

$$158 \quad v_{ij}(\xi) = \sum_{u=1}^n \omega_u \cdot [Y_{iu} - f_{iu}(\xi)] \cdot [Y_{ju} - f_{ju}(\xi)] \quad (2)$$

159 where,  $\omega_u$  is the weight factor,  $Y_{iu}$  the experimental concentration or temperature and  $f_{iu}(\xi)$  the  
160 estimated value for response  $i$  and event  $u$ ;  $Y_{ju}$  the experimental concentration and  $f_{ju}(\xi)$  the estimated  
161 value for response  $j$  and event  $u$ .

162

163 A modified Arrhenius equation was used to decrease the correlation between the pre-exponential  
 164 factor and the activation energy by linearizing the original Arrhenius equation as

$$165 \quad k(T) = \exp \left[ \ln \left( k(T_{ref}) \right) + \frac{E_a}{R \cdot T_{ref}} \cdot \left( 1 - \frac{T_{ref}}{T} \right) \right] \quad (3)$$

166 where,  $T_{ref}$  is the reference temperature chosen in the considered experimental temperature range.

167 Table 2 shows the experimental matrix for the regression and Table 3 shows the experimental matrix  
 168 for the validation stage.

169 Table 2. Experimental matrix for regression with initial conditions.

Run	P (bar)	m <sub>0</sub> BL (kg)	m <sub>0</sub> GVL (kg)	m <sub>0</sub> Ru (kg)	C <sub>p0</sub> (Jkg <sup>-1</sup> K <sup>-1</sup> )	UA <sub>0</sub> (WK <sup>-1</sup> )	[BL] <sub>0</sub> (molm <sup>-3</sup> )	[BHP] <sub>0</sub> (molm <sup>-3</sup> )	[GVL] <sub>0</sub> (molm <sup>-3</sup> )	[BuOH] <sub>0</sub> (molm <sup>-3</sup> )	Tr <sub>0</sub> (K)	Thermal mode
1	35	0.415	0.105	0.005	2736	17	4712	0	2082	29	393	isothermal
2	35	0.500	0.000	0.007	2736	19	5929	0	28	65	423	isothermal
3	35	0.500	0.000	0.007	2736	19	9	2222	3909	2883	432	isothermal
4	15	0.117	0.402	0.004	2736	17	1359	2	8198	8	403	isothermal
5	20	0.520	0.000	0.006	3131	17	6105	0	4	3	394	isothermal
1	22	0.500	0.000	0.005	2755	18	6114	0	0	0	412	isoperibolic
2	30	0.400	0.100	0.005	2773	17	4963	0	2079	0	392	isoperibolic
3	30	0.420	0.100	0.005	2646	17	4713	1	1853	31	403	isoperibolic
4	35	0.420	0.100	0.008	3131	17	5090	1	2040	3	393	isoperibolic
1	36	0.520	0.000	0.006	2751	17	5816	0	0	0	393	adiabatic
2	35	0.520	0.000	0.006	2789	15	6056	0	3	53	373	adiabatic
3	25	0.520	0.000	0.005	2704	15	5360	0	0	0	373	adiabatic
4	35	0.420	0.100	0.007	2624	15	4553	0	1786	31	373	adiabatic
5	25	0.520	0.000	0.006	2705	16	5635	0	20	37	383	adiabatic
6	30	0.350	0.170	0.008	2705	17	4223	4	3384	25	403	adiabatic
7	25	0.400	0.120	0.005	3131	18	4681	10	2337	30	413	adiabatic
8	20	0.520	0.000	0.004	3131	17	6339	0	8	62	403	adiabatic

170

171

172

173

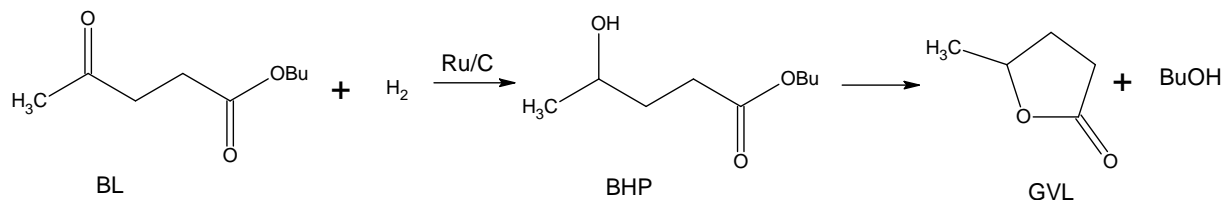
Table 3. Experimental matrix with initial conditions for validation

Run	P (bar)	$m_{0BL}$ (kg)	$m_{0GVL}$ (kg)	$m_{0Ru}$ (kg)	$C_{p0}$ (Jkg <sup>-1</sup> K <sup>-1</sup> )	$UA_0$ (WK <sup>-1</sup> )	$[BL]_0$ (molm <sup>-3</sup> )	$[BHP]_0$ (molm <sup>-3</sup> )	$[GVL]_0$ (molm <sup>-3</sup> )	$[BuOH]_0$ (molm <sup>-3</sup> )	$T_{r0}$ (K)	Thermal mode
6	38	0.415	0.105	0.005	2736	17	1050	2202	3482	1356	403	isothermal
7	35	0.415	0.105	0.005	2736	15	5059	0	2092	0	373	isothermal
8	20	0.520	0.000	0.006	2736	16	5756	0	4	34	384	isothermal
5	35	0.520	0.000	0.007	2788	15	5857	0	0	0	373	isoperibolic
6	35	0.420	0.100	0.008	2728	16	4984	1	1993	33	383	isoperibolic

176 3. Results and discussion

177 3.1. Kinetics

178 The global kinetics for the hydrogenation of BL is a two-step reaction (Fig. 2).



180 Fig. 2. Reaction pathway for the hydrogenation of BL over Ru/C.

181 The hydrogenation of the carbonyl group can take different routes, as illustrated in a previous article of  
182 our group [105]. In this work we considered five kinetic models to determine the most reliable, these  
183 kinetic models are described below:

- 184
- 185 • Eley-Rideal (ER1): This kinetic model considers that only BL is adsorbed into active sites of the  
186 catalyst, and then molecular hydrogen collides directly to the adsorbed BL.
  - 187 • Langmuir Hinshelwood with molecular adsorption of H<sub>2</sub> (LH1): This kinetic model considers that  
188 all reactants, BL and molecular hydrogen, are adsorbed into the active sites of the catalyst without  
189 dissociation, then the chemical reaction takes place between adsorbed molecules.
  - 190 • Langmuir Hinshelwood with hydrogen dissociation (LH2): As LH1 this kinetic model considers  
191 that all reactants, BL and molecular hydrogen, are adsorbed into the active sites of the catalyst.  
192 However, in this case, molecular hydrogen is dissociated into atomic hydrogen; then the chemical  
193 reaction takes place between adsorbed BL and adsorbed atomic hydrogen.
  - 194 • Non-competitive Langmuir Hinshelwood with molecular adsorption of H<sub>2</sub> (NCLH1): This kinetic  
195 model considers that there is no competition between the reactants for the active sites of the catalyst,  
196 so that it is considered that BL and molecular hydrogen are adsorbed in different active sites.  
197 Chemical reaction occurs between adsorbed BL and adsorbed molecular hydrogen without  
198 dissociation.
  - 199 • Non-competitive Langmuir Hinshelwood with hydrogen dissociation (NCLH2): As NCLH1 this  
kinetic model consider that there is no competition between the reactants. BL and molecular



200 hydrogen are adsorbed into different active sites, then the adsorbed molecular hydrogen is  
 201 dissociated into atomic hydrogen. The chemical reaction occurs between adsorbed BL and adsorbed  
 202 atomic hydrogen.

203 Table 4 shows the rate expression for the different possible reaction mechanisms.

204

205 Table 4. Kinetic expression for the different mechanisms for the hydrogenation step.

Kinetic model	Rate expression
Eley-Rideal with no adsorption of hydrogen (ER1)	$\frac{k_1 \cdot [H_2] \cdot K_{BL} \cdot [BL] \cdot \omega_{Cat.}}{(K_{BL} \cdot [BL] + K_{BHP} \cdot [BHP] + 1)}$
Langmuir Hinshelwood with molecular adsorption of H <sub>2</sub> (LH1)	$\frac{k_1 \cdot K_{H_2} \cdot [H_2] \cdot K_{BL} \cdot [BL] \cdot \omega_{Cat.}}{(K_{H_2} \cdot [H_2] + K_{BL} \cdot [BL] + K_{BHP} \cdot [BHP] + 1)^2}$
Langmuir Hinshelwood with hydrogen dissociation (LH2)	$\frac{k_1 \cdot K_H \cdot [H_2] \cdot K_i \cdot K_{BL} \cdot [BL] \cdot \omega_{Cat.}}{(\sqrt{K_H \cdot [H_2]} + K_{BL} \cdot [BL] + K_{BHP} \cdot [BHP] + K_i \cdot K_{BL} \cdot [BL] \cdot \sqrt{K_H \cdot [H_2]} + 1)^2}$
Non-competitive Langmuir Hinshelwood with no dissociation of hydrogen (NCLH1)	$\frac{k_1 \cdot K_{H_2} \cdot [H_2]}{(1 + K_{H_2} \cdot [H_2])} \cdot \frac{K_{BL} \cdot [BL]}{(1 + K_{BHP} \cdot [BHP] + K_{BL} \cdot [BL])} \cdot \omega_{Cat.}$
Non-competitive Langmuir Hinshelwood with hydrogen dissociation (NCLH2)	$\frac{k_1 \cdot K_H \cdot K_C \cdot K_{BL} \cdot [H_2]}{\sqrt{K_H \cdot [H_2]} + 1} \cdot \frac{[BL] \cdot \omega_{Cat.}}{K_{BL} \cdot [BL] + K_C \cdot \sqrt{K_H \cdot [H_2]} \cdot K_{BL} \cdot [BL] + K_{BHP} \cdot [BHP] + 1}$

206

207 The kinetic expression for the second reaction step, i.e., the cyclization step, was expressed as

$$208 \quad R_{Cyclization} = k_2 \cdot [BHP] \quad (4)$$

209 We applied linearization on the rate constant, and kinetic factors are displayed in Table 5.

210

211

Table 5. Kinetic factors and estimated parameters.

Models	Kinetic factors	Estimated parameters
ER1	$\exp\left(\ln(K_{BL}) + \ln(k_1(T_{ref})) + \frac{E_{a1}}{R \cdot T_{ref}} \cdot \left(1 - \frac{T_{ref}}{T}\right)\right)$	$\ln(K_{BL}),$ $\ln(k_1(T_{ref})), \frac{E_{a1}}{R \cdot T_{ref}}$ and $\ln(K_{BHP})$
LH1	$\exp\left(\ln(K_{H2}) + \ln(K_{BL}) + \ln(k_1(T_{ref})) + \frac{E_{a1}}{R \cdot T_{ref}} \cdot \left(1 - \frac{T_{ref}}{T}\right)\right)$	$\ln(K_{H2}), \ln(K_{BL}),$ $\ln(k_1(T_{ref})), \frac{E_{a1}}{R \cdot T_{ref}}$ and $\ln(K_{BHP})$
LH2	$\exp\left(\ln(K_H) + \ln(K_{BL}) + \ln(K_i) + \ln(k_1(T_{ref})) + \frac{E_{a1}}{R \cdot T_{ref}} \cdot \left(1 - \frac{T_{ref}}{T}\right)\right)$	$\ln(K_H), \ln(K_{BL}), \ln(K_i),$ $\ln(k_1(T_{ref})), \frac{E_{a1}}{R \cdot T_{ref}}$ and $\ln(K_{BHP})$
NCLH1	$\exp\left(\ln(K_{H2}) + \ln(K_{BL}^{\wedge}) + \ln(k_1(T_{ref})) + \frac{E_{a1}}{R \cdot T_{ref}} \cdot \left(1 - \frac{T_{ref}}{T}\right)\right)$	$\ln(K_{H2}), \ln(K_{BL}^{\wedge}), \ln(K_{BHP}^{\wedge}),$ $\ln(k_1(T_{ref}))$ and $\frac{E_{a1}}{R \cdot T_{ref}}$
NCLH2	$\exp\left(\ln(K_H) + \ln(K_{BL}^{\wedge}) + \ln(K_c) + \ln(k_1(T_{ref})) + \frac{E_{a1}}{R \cdot T_{ref}} \cdot \left(1 - \frac{T_{ref}}{T}\right)\right)$	$\ln(K_H), \ln(K_{BL}^{\wedge}), \ln(K_{BHP}^{\wedge}),$ $\ln(K_c),$ $\ln(k_1(T_{ref}))$ and $\frac{E_{a1}}{R \cdot T_{ref}}$

214 3.2. Material and energy balances

215 Due to the vigorous stirring, ideal hydrodynamics was assumed in the RC1 reactor. Material balances  
 216 for different compounds in the liquid phase leads to:

$$217 \frac{dC_{BL}}{dt} = -R_{Hydrogenation} \quad (5)$$

$$218 \frac{d[H_2]_{liq}}{dt} = k_L \cdot a \cdot ([H_2]_{liq}^* - [H_2]_{liq}) - R_{Hydrogenation} \quad (6)$$

$$219 \frac{dC_{BHP}}{dt} = R_{Hydrogenation} - R_{Cyclization} \quad (7)$$

$$220 \frac{dC_{BuOH}}{dt} = R_{Cyclization} \quad (8)$$

$$221 \frac{dC_{GVL}}{dt} = R_{Cyclization} \quad (9)$$

222 The term  $[H_2]_{liq}^*$  is hydrogen concentration at the gas-liquid interface. This value depends on  
 223 temperature and was determined through Henry's constant:  $He(T) = \frac{[H_2]_{liq}^*}{P_{H_2,Reactor}}$  [54]. A separate mass  
 224 transfer coefficient study was carried out to estimate the volumetric gas-to-liquid mass transfer  
 225 coefficient for hydrogen. A similar methodology applied in a previous study of our group was used [57]  
 226 to estimate this mass transfer coefficient by taking into account density and viscosity of the reaction  
 227 mixture [106]. For the sake of clarity, this information was added in Supplementary Material (S1). The  
 228 value of  $He(T)$  can change with temperature and chemical composition, the results from Capecci et al.  
 229 were used [54].

230 The heat balance equation for the liquid phase leads to

$$231 \frac{dT_R}{dt} = \frac{(-R_{Hydrogenation} \cdot \Delta H_{R,Hydrogenation} \cdot V - R_{Cyclization} \cdot \Delta H_{R,Cyclization} \cdot V) + UA \cdot (T_j - T_R) + \alpha \cdot (T_{amb} - T_R)}{m_R \cdot C_{PR} + m_{insert} \cdot C_{pinsert} + m_{catalyst} \cdot C_{p catalyst}} \quad (10)$$

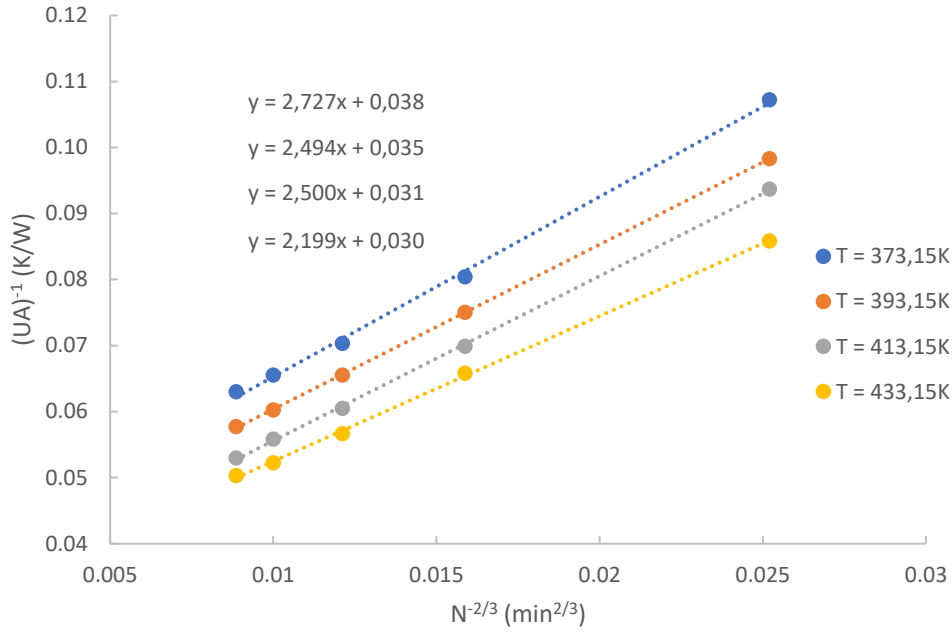
232 The term  $\alpha \cdot (T_{amb} - T_R)$  represents the heat loss with the surroundings. The term  $UA \cdot (T_j - T_R)$  is the  
 233 heat flow rate exchanged with the heat carrier, and UA is the global heat transfer,  $T_j$  and  $T_R$  are the jacket  
 234 and reaction temperatures. The term  $m_R \cdot C_{PR} + m_{insert} \cdot C_{pinsert} + m_{catalyst} \cdot C_{p catalyst}$  represents the

235 thermal inertia, where  $m_{insert} \cdot Cp_{insert}$  is equal to  $52 \text{ J}\cdot\text{K}^{-1}$ , according to the manufacturer,  $Cp_R$  was  
236 evaluated based on the evolution of chemical composition and temperature [24] and  $Cp_{catalyst}$  was  
237 found based on the article of Lu et al. [107]. Reaction enthalpies for hydrogenation  $\Delta H_{R,Hydrogenation}$   
238 and cyclization  $\Delta H_{R,Cyclization}$  were the ones calculated by Wang et al. [46].

239

240 3.3. Calibration results (Wilson plot)

241 In order to verify the thin wall approximation between the heat carrier and reaction mixture and to  
 242 predict the UA values with reaction temperature, UA value was calculated at different temperatures and  
 243 rotating speeds in the absence of reaction, i.e., Wilson plot [98]. Fig. 3 shows the linearity between 1/UA  
 244 and  $N^{-2/3}$ , confirming the thin wall approximation.



245  
 246 Fig. 3. Wilson plot.

247 3.4. Gas-liquid mass transfer results

248 In these experiments, rates of hydrogenation and cyclization are equal to zero, thus one should integrate  
 249 Eq. (6) to estimate the  $k_L a$  value. The volumetric mass transfer coefficient was expressed as [57]:

$$250 \quad k_L a = (k_L a)_{modified} \cdot \left(\frac{T_{liq}}{\mu_{liq}}\right)^{0.5} \cdot \left(\frac{\rho_{liq}}{\mu_{liq}}\right)^{0.25} \quad (11)$$

251 The constant  $(k_L a)_{modified}$  was calculated from experiments shown in Table 1 as described in  
 252 Supplementary Material (S1). From Table S1.1, one can notice that the calculated value of  
 253  $(k_L a)_{modified}$  for each run is very similar. The average value of  $(k_L a)_{modified}$  was found to be  $2.25 \cdot 10^{-6}$   
 254  $(\text{Pa}\cdot\text{s}\cdot\text{K}^{-1})^{0.5}(\text{Pa}\cdot\text{s}\cdot\text{kg}^{-1}\cdot\text{m}^{-3})^{0.25}\cdot\text{s}^{-1}$  and the standard deviation was equal to  $0.14 (\text{Pa}\cdot\text{s}\cdot\text{K}^{-1})^{0.5}(\text{Pa}\cdot\text{s}\cdot\text{kg}^{-1}\cdot\text{m}^{-3})^{0.25}$   
 255  $\cdot\text{s}^{-1}$ . This value was found to be similar than the one of Wang et al. [57].

256 3.5. Kinetic modeling

257 3.5.1. Regression

258 The five models were tested during the regression (ER1, LH1, LH2, NCLH1 and NCLH2). The Akaike  
 259 information criterion (AIC) was used to evaluate the most reliable models, and it was calculated as

$$260 \text{ AIC: } \textit{number of independant event} \cdot \ln \left( \frac{[Y_{ju} - f_{ju}(\xi)]^2}{\textit{number of independant event}} \right) +$$

$$261 \text{ 2. } \textit{Number of estimated parameters} \tag{12}$$

262

263 This criterion penalizes models with numerous parameters to estimate. Table 6 shows the values for  
 264 each observable.

265 Table 6. AIC values for each observable and model.

	AIC				Number of parameters to estimate
	BL	BHP	GVL	Tr	
ER1	2529	2010	2151	36	6
LH1	2498	2008	2131	117	7
LH2	2500	2010	2133	118	8
NCLH1	2520	1993	2139	54	7
NCLH2	2508	2056	2161	38	8

266

267 Table 6 shows that NCLH1 and NCLH2 are the most reliable model by considering the AIC for all  
 268 observables. Indeed, NCLH1 and NCLH2 models present a good compromise between the lowest AIC  
 269 values for Tr and medium AIC values for BL, BHP and GVL.

270 For the sake of clarity, modeling results using NCLH1 model are displayed, and the others are in  
 271 Supplementary Material (S2). Table 7 shows the value of the estimated parameters and the statistical  
 272 values. The model can estimate the kinetic constants with low credible intervals. However, the  
 273 estimation of adsorption constants is more challenging due to the difficulty to estimate such  
 274 thermodynamic constants.

275

276

Table 7. Estimated values at  $T_{ref} = 398.15$  K and statistical data for NCLH1.

	Units	Estimate	HPD	HPD%
$\ln(k_1(T_{ref}))$	mol. kg_dry basis $\text{RuC}^{-1} \cdot \text{s}^{-1}$	5.34	0.12	2.17
$\ln(k_2(T_{ref}))$	$\text{s}^{-1}$	-10.19	0.03	0.28
$\frac{E_{a1}}{R \cdot T_{ref}}$	-	9.25	0.73	7.92
$\frac{E_{a2}}{R \cdot T_{ref}}$	-	8.09	0.59	7.27
$\ln(K_H)$	$\text{m}^3 \cdot \text{mol}^{-1}$	-2.91	0.26	8.93
$\ln(K_{BL}^{\wedge})$	$\text{m}^3 \cdot \text{mol}^{-1}$	0.011	-	
$\ln(K_{BHP}^{\wedge})$	$\text{m}^3 \cdot \text{mol}^{-1}$	7.961	-	

277

278

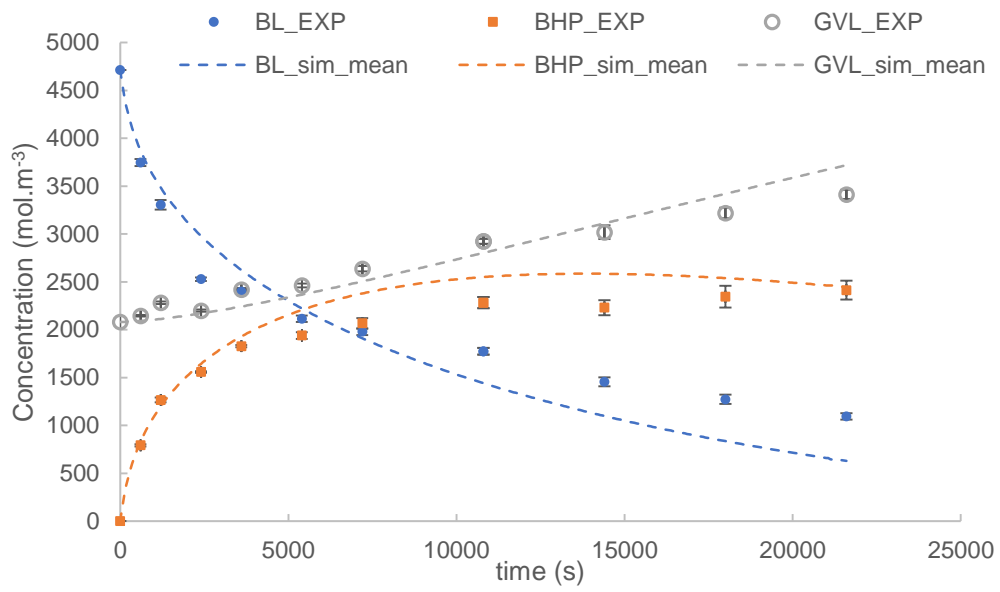
Table 8. Normalized parameter covariance matrix for NCLH1.

	$\ln(k_1(T_{ref}))$	$\ln(k_2(T_{ref}))$	$\frac{E_{a1}}{R \cdot T_{ref}}$	$\frac{E_{a2}}{R \cdot T_{ref}}$	$\ln(K_H)$
$\ln(k_1(T_{ref}))$	1				
$\ln(k_2(T_{ref}))$	0.07	1			
$\frac{E_{a1}}{R \cdot T_{ref}}$	-0.163	-0.047	1		
$\frac{E_{a2}}{R \cdot T_{ref}}$	-0.086	-0.671	-0.059	1	
$\ln(K_H)$	-0.981	-0.071	0.123	0.081	1

279

280 Correlation between the majority of estimated parameters are lower than 0.90 in absolute value, thus  
 281 one can consider that the estimated parameters are not correlated [108]. This absence of correlation  
 282 shows that the parameters are well identified. The parameter  $\ln(k_1(T_{ref}))$  and  $\ln(K_H)$  are strongly  
 283 correlated, due to the difficulty to correctly track the hydrogenation rate.

284 Figs 4-6 show the fit of the model to experimental data in different thermal modes for NCLH1 model.  
 285 Generally, the model fits well the experimental data in these modes as it is confirmed with the parity  
 286 plot (Fig. 7). In isothermal mode, experimental temperatures were not considered in the objective  
 287 function, because the reaction temperature is stable along the reaction course. For adiabatic and  
 288 isoperibolic experiments, we measured concentrations at the beginning and at the end of the reaction.



289

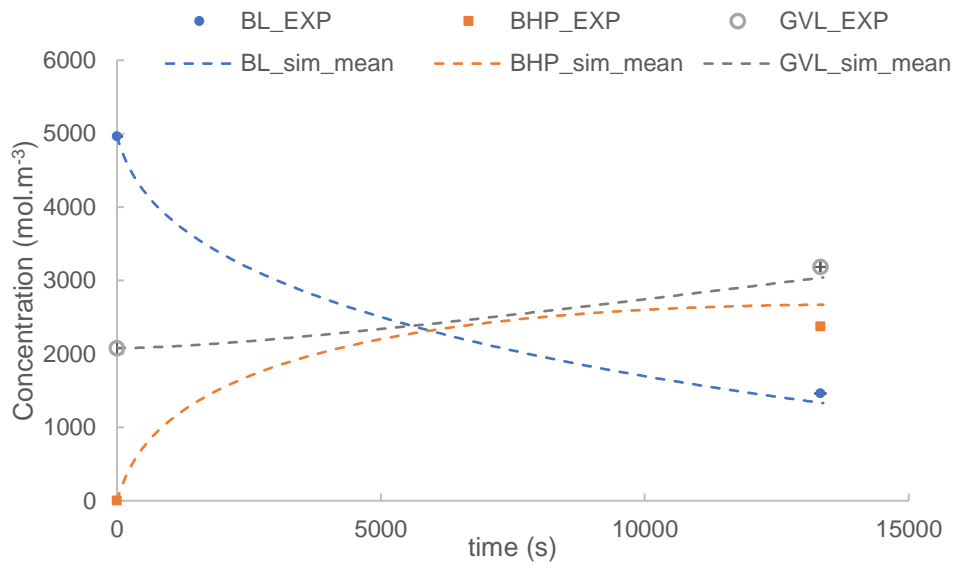
290

291

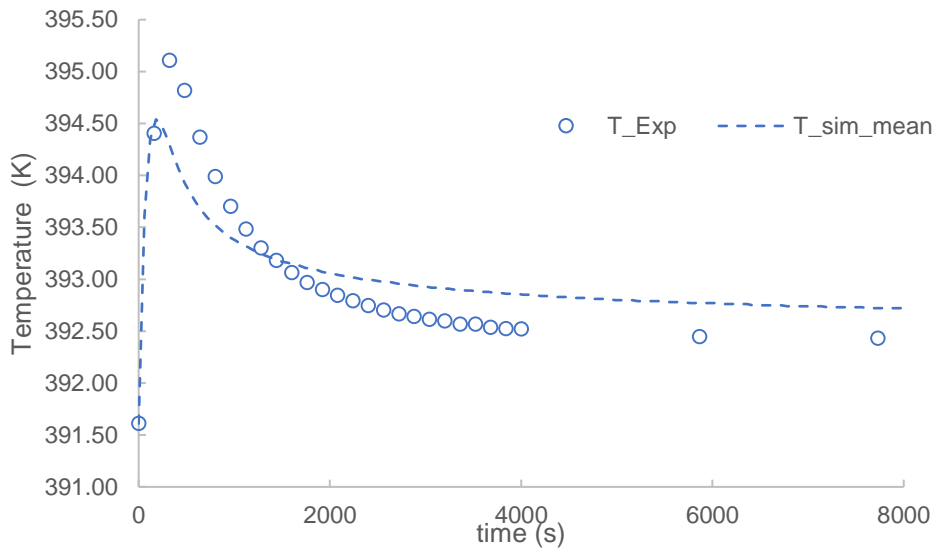
Fig. 4. Fit of the NCLH1 model to isothermal experimental data for Run 1.



292



293



294

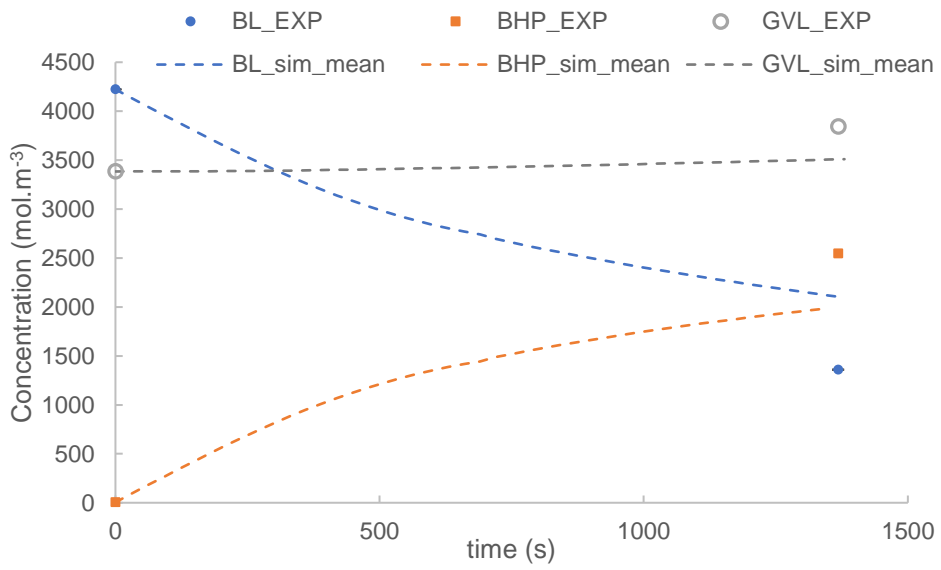
295

Fig. 5. Fit of the NCLH1 model to isoperibolic experimental data for Run 2.

296

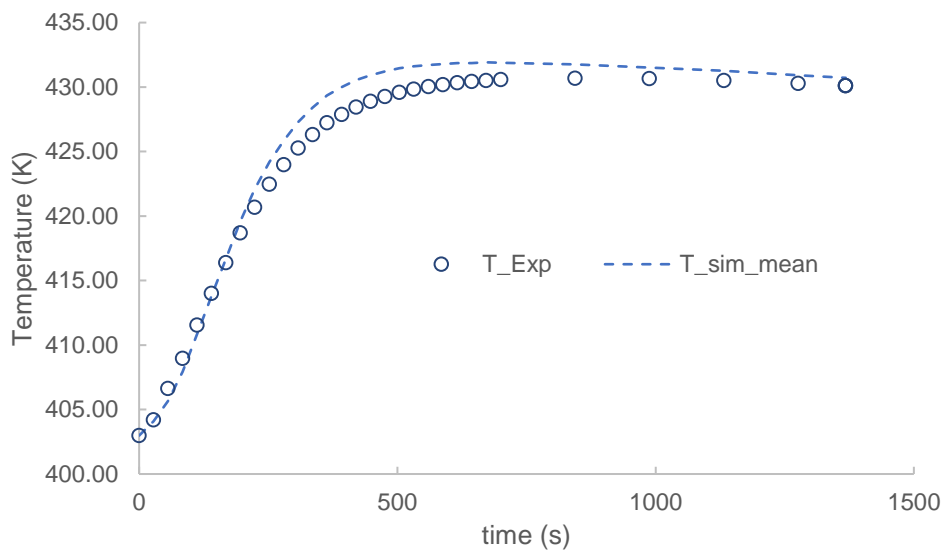
297

298



299

300



301

302

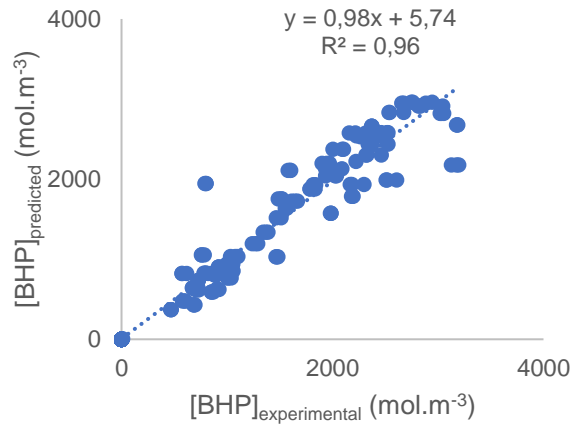
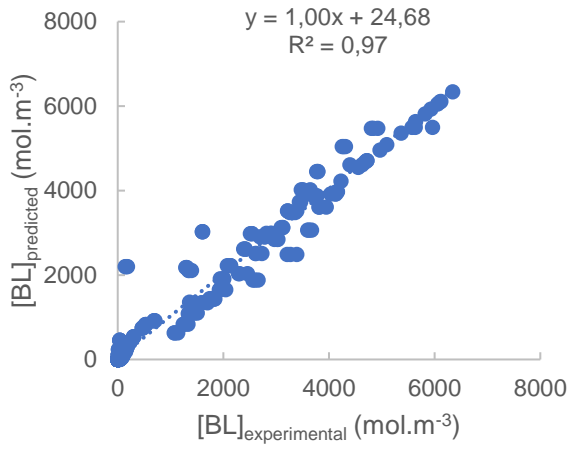
303

304

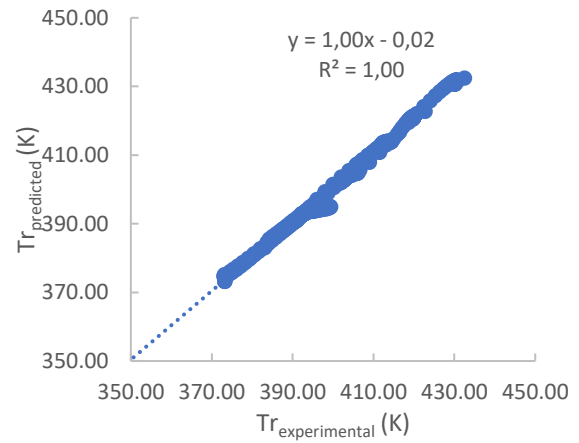
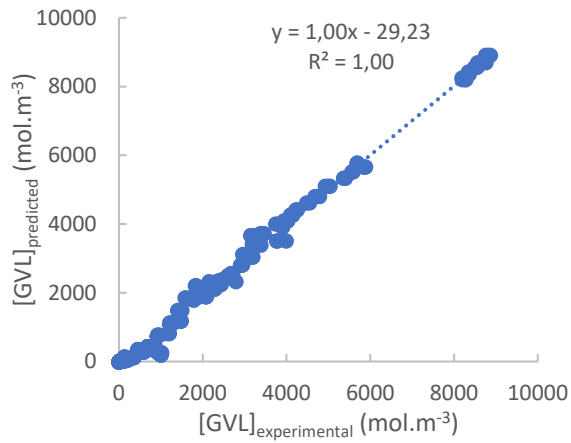
305

306

Fig. 6. Fit of the NCLH2 model to adiabatic experimental data for Run 6.



307



308

309

Fig. 7. Parity plots from regression stage (model NCLH1)

310 3.5.2. Validation stage

311 A holdout validation method was used. The estimated kinetic and thermodynamic constants obtained  
312 from the regression stage were used to predict the kinetic profile by using initial experimental conditions  
313 from Table 3. Fig. 8 show parity plots for the validation experiments for NCLH1, showing the good  
314 prediction capacity of NCLH1. NCLH1 can correctly predict BL and GVL concentrations, as well as  
315 reaction temperature. This model is less accurate for BHP concentration.

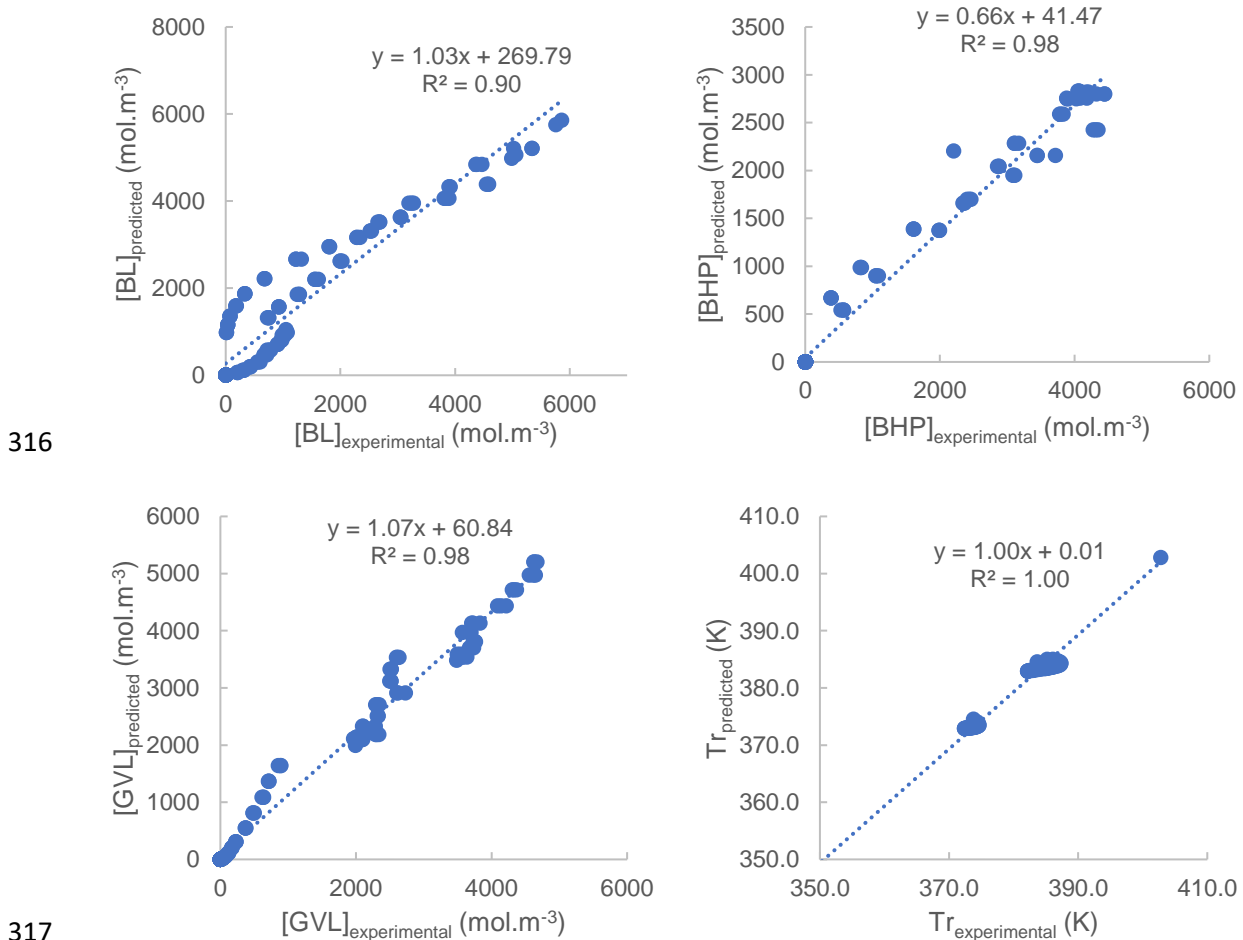


Fig. 8. Parity plots from validation stage (model NCLH1)

#### 320 4. Conclusions

321 There is a need to develop reliable and robust kinetic models to scaleup, optimize process production,  
322 energy consumption and production, cost production and for thermal risk assessment. Traditionally,  
323 these types of kinetic models are developed in isothermal conditions without considering the energy  
324 balance. Thus, such models are limited for energy optimization or thermal risk assessment.

325 In this work, we developed and assessed 5 kinetic models in different thermal modes, i.e., isothermal,  
326 adiabatic and isoperibolic one. We applied this approach for the production of  $\gamma$ -valerolactone from the  
327 hydrogenation of butyl levulinate. To the best of the authors' knowledge, it is the first time that kinetic  
328 model are done in different thermal modes. Such models can provide crucial information in process  
329 optimization, scaleup, energy recovery for pinch analysis and thermal risk assessment.

330 Kinetic experiments were performed by using high concentrated solution of BL in the RC1 calorimeter  
331 using three thermal modes (isothermal, isoperibolic and adiabatic). For the regression stage, we varied  
332 the initial temperature from 383 to 430 K, catalyst loading from 6.5 to 13.5 kg/m<sup>3</sup> and hydrogen pressure  
333 from 15 to 35 bar. We were able to estimate kinetic constants for 5 kinetic models: Eley-Rideal with no  
334 adsorption of hydrogen (ER1), Langmuir Hinshelwood with molecular adsorption of H<sub>2</sub> (LH1),  
335 Langmuir Hinshelwood with hydrogen dissociation (LH2), Non-competitive Langmuir Hinshelwood  
336 with no dissociation of hydrogen (NCLH1) and Non-competitive Langmuir Hinshelwood with hydrogen  
337 dissociation (NCLH2). From the AIC criterion, we found that NCLH1 and NCLH2 models were the  
338 most reliable model. A validation stage was done using a holdout method, and confirmed the reliability  
339 of NCLH1 model.

340 A continuation of this work could be the determination of these constants from quantum mechanics  
341 method.

342

343 **Acknowledgments**

344 This investigation was carried out in the framework of the ARBRE project (Risk Analysis to processes  
345 valorizing 2nd generation biomass and using Renewable energies). ARBRE is cofounded by European  
346 Union through the European Regional Development Fund (agreement n° 00130305) and by Normandy  
347 Region (agreement n° 21E05304), via the support of "pôle CTM (Continuum Terre-Mer) and EP2M  
348 (Énergies, Propulsion, Matière, Matériaux) de Normandie université". The authors thank the Ministry  
349 of High Education, Science and Technology of Dominican Republic (MESCYT).

350 For the analytical part, this work has been partially supported by University of Rouen Normandy, INSA  
351 Rouen Normandy, the Centre National de la Recherche Scientifique (CNRS), European Regional  
352 Development Fund (ERDF) N° HN0001343, Labex SynOrg (ANR-11-LABX-0029), Carnot Institute  
353 I2C, the graduate school for reasearch XL-Chem (ANR-18-EURE-0020 XL CHEM) and by Region  
354 Normandie. GC was financed by FEDER RIN Green Chem 2019NU01FOBC08 Number: 17P04374.

355 **References**

- 356 [1] Rapier R. Highlights From The BP Statistical Review Of World Energy 2021 2021.  
357 [https://sourcezon.com/articles/highlights-from-the-bp-statistical-review-of-world-energy-](https://sourcezon.com/articles/highlights-from-the-bp-statistical-review-of-world-energy-2021?slug=highlights-from-the-bp-statistical-review-of-world-energy-2021&q=)  
358 [2021?slug=highlights-from-the-bp-statistical-review-of-world-energy-2021&q=](https://sourcezon.com/articles/highlights-from-the-bp-statistical-review-of-world-energy-2021?slug=highlights-from-the-bp-statistical-review-of-world-energy-2021&q=) (accessed  
359 February 5, 2023).
- 360 [2] Manikandan S, Vickram S, Sirohi R, Subbaiya R, Krishnan RY, Karmegam N, et al. Critical  
361 review of biochemical pathways to transformation of waste and biomass into bioenergy.  
362 *Bioresour Technol* 2023;372:128679. <https://doi.org/10.1016/j.biortech.2023.128679>.
- 363 [3] Amerit B, Ntayi JM, Ngoma M, Bashir H, Echegu S, Nantongo M. Commercialization of  
364 biofuel products: A systematic literature review. *Renew Energy Focus* 2023;44:223–36.  
365 <https://doi.org/10.1016/j.ref.2022.12.008>.
- 366 [4] Jiang Y, Li Z, Li Y, Chen L, Zhang H, Li H, et al. Recent advances in sustainable catalytic  
367 production of 5-methyl-2-pyrrolidones from bio-derived levulinate. *Fuel* 2023;334:126629.  
368 <https://doi.org/10.1016/j.fuel.2022.126629>.
- 369 [5] Ashokkumar V, Venkatkarthick R, Jayashree S, Chuetor S, Dharmaraj S, Kumar G, et al.  
370 Recent advances in lignocellulosic biomass for biofuels and value-added bioproducts - A  
371 critical review. *Bioresour Technol* 2022;344:960–8524.  
372 <https://doi.org/10.1016/j.biortech.2021.126195>.
- 373 [6] Liu WJ, Yu HQ. Thermochemical Conversion of Lignocellulosic Biomass into Mass-  
374 Producible Fuels: Emerging Technology Progress and Environmental Sustainability  
375 Evaluation. *ACS Environ Au* 2022;2:98–114. <https://doi.org/10.1021/acsenvironau.1c00025>.
- 376 [7] Jamil F, Saleem M, Ali Qamar O, Khurram MS, Al-Muhtaseb AH, Inayat A, et al. State-of-the-  
377 art catalysts for clean fuel (methyl esters) production—a comprehensive review. *JPhys Energy*  
378 2023;5:014005. <https://doi.org/10.1088/2515-7655/aca5b3>.
- 379 [8] Tomei J, Helliwell R. Food versus fuel? Going beyond biofuels. *Land Use Policy*

- 380 2016;56:320–6. <https://doi.org/10.1016/j.landusepol.2015.11.015>.
- 381 [9] Alonso DM, Wettstein SG, Mellmer MA, Gurbuz EI, Dumesic JA. Integrated conversion of  
382 hemicellulose and cellulose from lignocellulosic biomass. *Energy Environ Sci* 2013;6:76–80.  
383 <https://doi.org/10.1039/c2ee23617f>.
- 384 [10] Li G, Liu W, Ye C, Li X, Si CL. Chemocatalytic Conversion of Cellulose into Key Platform  
385 Chemicals. *Int J Polym Sci* 2018;2018. <https://doi.org/10.1155/2018/4723573>.
- 386 [11] Guo K, Guan Q, Xu J, Tan W. Mechanism of Preparation of Platform Compounds from  
387 Lignocellulosic Biomass Liquefaction Catalyzed by Bronsted Acid: A Review. *J Bioresour*  
388 *Bioprod* 2019;4:202–13. <https://doi.org/10.12162/jbb.v4i4.009>.
- 389 [12] Di Menno Di Bucchianico D, Wang Y, Buvat JC, Pan Y, Casson Moreno V, Leveneur S.  
390 Production of levulinic acid and alkyl levulinates: A process insight. *Green Chem*  
391 2022;24:614–46. <https://doi.org/10.1039/d1gc02457d>.
- 392 [13] Yan K, Yang Y, Chai J, Lu Y. Catalytic reactions of gamma-valerolactone: A platform to fuels  
393 and value-added chemicals. *Appl Catal B Environ* 2015;179:292–304.  
394 <https://doi.org/10.1016/J.APCATB.2015.04.030>.
- 395 [14] Kerkel F, Markiewicz M, Stolte S, Müller E, Kunz W. The green platform molecule gamma-  
396 valerolactone - ecotoxicity, biodegradability, solvent properties, and potential applications.  
397 *Green Chem* 2021;23:2962–76. <https://doi.org/10.1039/d0gc04353b>.
- 398 [15] Qu R, Junge K, Beller M. Hydrogenation of Carboxylic Acids, Esters, and Related Compounds  
399 over Heterogeneous Catalysts: A Step toward Sustainable and Carbon-Neutral Processes.  
400 *Chem Rev* 2022. <https://doi.org/10.1021/acs.chemrev.2c00550>.
- 401 [16] Di Menno Di Bucchianico D, Buvat JC, Mignot M, Casson Moreno V, Leveneur S. Role of  
402 solvent the production of butyl levulinate from fructose. *Fuel* 2022;318:123703.  
403 <https://doi.org/10.1016/j.fuel.2022.123703>.
- 404 [17] Liu C, Wei M, Wang J, Xu J, Jiang J, Wang K. Facile Directional Conversion of Cellulose and



- 405 Bamboo Meal Wastes over Low-Cost Sulfate and Polar Aprotic Solvent. *ACS Sustain Chem*  
406 *Eng* 2020;8:5776–86. <https://doi.org/10.1021/acssuschemeng.0c01280>.
- 407 [18] Wang S, Zhao Y, Lin H, Chen J, Zhu L, Luo Z. Conversion of C5 carbohydrates into furfural  
408 catalyzed by a Lewis acidic ionic liquid in renewable  $\gamma$ -valerolactone. *Green Chem*  
409 2017;19:3869–79. <https://doi.org/10.1039/c7gc01298e>.
- 410 [19] Chew AK, Walker TW, Shen Z, Demir B, Witteman L, Euclide J, et al. Effect of Mixed-  
411 Solvent Environments on the Selectivity of Acid-Catalyzed Dehydration Reactions. *ACS Catal*  
412 2020;10:1679–91. <https://doi.org/10.1021/acscatal.9b03460>.
- 413 [20] Kang D, Choi M, Kim D, Han J. Environmental Analysis of Catalytic Adipic Acid Production  
414 Strategies from Two Different Lignocellulosic Biomasses. *ACS Sustain Chem Eng* 2022.  
415 <https://doi.org/10.1021/acssuschemeng.2c00070>.
- 416 [21] Motagamwala AH, Won W, Maravelias CT, Dumesic JA. An engineered solvent system for  
417 sugar production from lignocellulosic biomass using biomass derived  $\gamma$ -valerolactone. *Green*  
418 *Chem* 2016;18:5756–63. <https://doi.org/10.1039/c6gc02297a>.
- 419 [22] Baco S, Klinksiek M, Ismail Bedawi Zakaria R, Antonia Garcia-Hernandez E, Mignot M,  
420 Legros J, et al. Solvent effect investigation on the acid-catalyzed esterification of levulinic acid  
421 by ethanol aided by a Linear Solvation Energy Relationship. *Chem Eng Sci* 2022;260:117928.  
422 <https://doi.org/10.1016/j.ces.2022.117928>.
- 423 [23] Pokorný V, Štejfá V, Fulem M, Červinka C, Růžička K. Vapor Pressures and Thermophysical  
424 Properties of Ethylene Carbonate, Propylene Carbonate,  $\gamma$ -Valerolactone, and  $\gamma$ -Butyrolactone.  
425 *J Chem Eng Data* 2017;62:4174–86. <https://doi.org/10.1021/acs.jced.7b00578>.
- 426 [24] Ariba H, Wang Y, Devouge-Boyer C, Stateva RP, Leveneur S. Physicochemical Properties for  
427 the Reaction Systems: Levulinic Acid, Its Esters, and  $\gamma$ -Valerolactone. *J Chem Eng Data*  
428 2020;65:3008–20. <https://doi.org/10.1021/acs.jced.9b00965>.
- 429 [25] Horváth IT, Mehdi H, Fábos V, Boda L, Mika LT.  $\gamma$ -Valerolactone—a sustainable liquid for

- 430 energy and carbon-based chemicals. *Green Chem* 2008;10:238–24.  
431 <https://doi.org/10.1039/b712863k>.
- 432 [26] Raj T, Chandrasekhar K, Banu R, Yoon JJ, Kumar G, Kim SH. Synthesis of  $\gamma$ -valerolactone  
433 (GVL) and their applications for lignocellulosic deconstruction for sustainable green  
434 biorefineries. *Fuel* 2021;303:121333. <https://doi.org/10.1016/j.fuel.2021.121333>.
- 435 [27] Al-Naji M, Puértolas B, Kumru B, Cruz D, Bäuml M, Schmidt BVKJ, et al. Sustainable  
436 Continuous Flow Valorization of  $\gamma$ -Valerolactone with Trioxane to  $\alpha$ -Methylene- $\gamma$ -  
437 Valerolactone over Basic Beta Zeolites. *ChemSusChem* 2019;12:2628–36.  
438 <https://doi.org/10.1002/cssc.201900418>.
- 439 [28] Manzer LE. Catalytic synthesis of  $\alpha$ -methylene- $\gamma$ -valerolactone: a biomass-derived acrylic  
440 monomer. *Appl Catal A Gen* 2004;272:249–56.  
441 <https://doi.org/10.1016/J.APCATA.2004.05.048>.
- 442 [29] Choi M, Byun J, Park H, Jeong K, Kim SM, Han J. Economically-feasible “greener”  
443 transformation of gamma-valerolactone to nylon 6,6. *Biomass and Bioenergy*  
444 2022;162:106503. <https://doi.org/10.1016/J.BIOMBIOE.2022.106503>.
- 445 [30] Hayes G, Laurel M, MacKinnon D, Zhao T, Houck HA, Becer CR. Polymers without  
446 Petrochemicals: Sustainable Routes to Conventional Monomers. *Chem Rev* 2022.  
447 <https://doi.org/10.1021/acs.chemrev.2c00354>.
- 448 [31] Alonso DM, Bond JQ, Dumesic JA. Catalytic conversion of biomass to biofuels. *Green Chem*  
449 2010;12:1493–513. <https://doi.org/10.1039/c004654j>.
- 450 [32] Dutta S, Yu IKM, Tsang DCW, Ng YH, Ok YS, Sherwood J, et al. Green synthesis of gamma-  
451 valerolactone (GVL) through hydrogenation of biomass-derived levulinic acid using non-noble  
452 metal catalysts: A critical review. *Chem Eng J* 2019;372:992–1006.  
453 <https://doi.org/10.1016/j.cej.2019.04.199>.
- 454 [33] Making alternative fuels cheaper | MIT News | Massachusetts Institute of Technology n.d.

- 455 <https://news.mit.edu/2013/making-alternative-fuels-cheaper-0617> (accessed February 5, 2023).
- 456 [34] Anagnostopoulou E, Lilas P, Diamantopoulou P, Fakas C, Krithinakis I, Patatsi E, et al.  
457 Hydrogenation of the pivotal biorefinery platform molecule levulinic acid into renewable fuel  
458  $\gamma$ -valerolactone catalyzed by unprecedented highly active and stable ruthenium nanoparticles in  
459 aqueous media. *Renew Energy* 2022;192:35–45. <https://doi.org/10.1016/j.renene.2022.04.081>.
- 460 [35] Kasar GB, Date NS, Bhosale PN, Rode C V. Steering the Ester and  $\gamma$ -Valerolactone  
461 Selectivities in Levulinic Acid Hydrogenation. *Energy and Fuels* 2018;32:6887–900.  
462 <https://doi.org/10.1021/acs.energyfuels.8b01263>.
- 463 [36] Alonso DM, Wettstein SG, Dumesic JA. Gamma-valerolactone, a sustainable platform  
464 molecule derived from lignocellulosic biomass. *Green Chem* 2013;15:584–95.  
465 <https://doi.org/10.1039/c3gc37065h>.
- 466 [37] Yan K, Lafleur T, Wu X, Chai J, Wu G, Xie X. Cascade upgrading of  $\gamma$ -valerolactone to  
467 biofuels. *Chem Commun* 2015;51:6984–7. <https://doi.org/10.1039/c5cc01463h>.
- 468 [38] Ayodele OO, Dawodu FA, Yan D, Dong H, Xin J, Zhang S. Production of Bio-Based Gasoline  
469 by Noble-Metal-Catalyzed Hydrodeoxygenation of  $\alpha$ -Angelica Lactone Derived Di/Trimers.  
470 *ChemistrySelect* 2017;2:4219–25. <https://doi.org/10.1002/slct.201700451>.
- 471 [39] Wang H, Wu Y, Guo S, Dong C, Ding M.  $\gamma$ -Valerolactone converting to butene via ring-  
472 opening and decarboxylation steps over amorphous SiO<sub>2</sub>-Al<sub>2</sub>O<sub>3</sub> catalyst. *Mol Catal*  
473 2020;497:111218. <https://doi.org/10.1016/j.mcat.2020.111218>.
- 474 [40] Wang H, Wu Y, Li Y, Peng J, Gu XK, Ding M. One-step synthesis of pentane fuel from  $\gamma$ -  
475 valerolactone with high selectivity over a Co/HZSM-5 bifunctional catalyst. *Green Chem*  
476 2021;23:4780–9. <https://doi.org/10.1039/d1gc01062j>.
- 477 [41] Bond JQ, Alonso DM, Wang D, West RM, Dumesic JA. Integrated catalytic conversion of  $\gamma$ -  
478 valerolactone to liquid alkenes for transportation fuels. *Science* (80- ) 2010;327:1110–4.  
479 <https://doi.org/10.1126/science.1184362>.

- 480 [42] Han J. Integrated process for simultaneous production of jet fuel range alkenes and N-  
481 methylformanilide using biomass-derived gamma-valerolactone. *J Ind Eng Chem*  
482 2017;48:173–9. <https://doi.org/10.1016/j.jiec.2016.12.036>.
- 483 [43] He J, Lin L, Liu M, Miao C, Wu Z, Chen R, et al. A durable Ni/La-Y catalyst for efficient  
484 hydrogenation of  $\gamma$ -valerolactone into pentanoic biofuels. *J Energy Chem* 2022;70:347–55.  
485 <https://doi.org/10.1016/j.jechem.2022.02.011>.
- 486 [44] Casson Moreno V, Garbetti AL, Leveneur S, Antonioni G. A consequences-based approach for  
487 the selection of relevant accident scenarios in emerging technologies. *Saf Sci* 2019;112:142–  
488 51. <https://doi.org/10.1016/j.ssci.2018.10.024>.
- 489 [45] Wang Y, Vernières-Hassimi L, Casson-Moreno V, Hébert JP, Leveneur S. Thermal Risk  
490 Assessment of Levulinic Acid Hydrogenation to  $\gamma$ -Valerolactone. *Org Process Res Dev*  
491 2018;22:1092–100. <https://doi.org/10.1021/acs.oprd.8b00122>.
- 492 [46] Wang Y, Plazl I, Vernières-Hassimi L, Leveneur S. From calorimetry to thermal risk  
493 assessment:  $\gamma$ -Valerolactone production from the hydrogenation of alkyl levulinates. *Process*  
494 *Saf Environ Prot* 2020;144:32–41. <https://doi.org/10.1016/j.psep.2020.07.017>.
- 495 [47] Karanwal N, Kurniawan RG, Park J, Verma D, Oh S, Kim SM, et al. One-pot, cascade  
496 conversion of cellulose to  $\gamma$ -valerolactone over a multifunctional Ru–Cu/zeolite-Y catalyst in  
497 supercritical methanol. *Appl Catal B Environ* 2022;314:121466.  
498 <https://doi.org/10.1016/j.apcatb.2022.121466>.
- 499 [48] Siddiqui N, Pendem C, Goyal R, Khatun R, Khan TS, Samanta C, et al. Study of  $\gamma$ -  
500 valerolactone production from hydrogenation of levulinic acid over nanostructured Pt-  
501 hydrotalcite catalysts at low temperature. *Fuel* 2022;323:124272.  
502 <https://doi.org/10.1016/j.fuel.2022.124272>.
- 503 [49] Mehdi H, Fábos V, Tuba R, Bodor A, Mika LT, Horváth IT. Integration of homogeneous and  
504 heterogeneous catalytic processes for a multi-step conversion of biomass: From sucrose to

- 505 levulinic acid,  $\gamma$ -valerolactone, 1,4-pentanediol, 2-methyl-tetrahydrofuran, and alkanes. *Top.*  
506 *Catal.*, vol. 48, Springer; 2008, p. 49–54. <https://doi.org/10.1007/s11244-008-9047-6>.
- 507 [50] Luo W, Deka U, Beale AM, Van Eck ERH, Bruijninx PCA, Weckhuysen BM. Ruthenium-  
508 catalyzed hydrogenation of levulinic acid: Influence of the support and solvent on catalyst  
509 selectivity and stability. *J Catal* 2013;301:175–86. <https://doi.org/10.1016/j.jcat.2013.02.003>.
- 510 [51] Hengne AM, Rode C V. Cu–ZrO<sub>2</sub> nanocomposite catalyst for selective hydrogenation of  
511 levulinic acid and its ester to  $\gamma$ -valerolactone. *Green Chem* 2012;14:1064–72.  
512 <https://doi.org/10.1039/c2gc16558a>.
- 513 [52] Piskun AS, van de Bovenkamp HH, Rasrendra CB, Winkelman JGM, Heeres HJ. Kinetic  
514 modeling of levulinic acid hydrogenation to  $\gamma$ -valerolactone in water using a carbon supported  
515 Ru catalyst. *Appl Catal A Gen* 2016;525:158–67. <https://doi.org/10.1016/j.apcata.2016.06.033>.
- 516 [53] Capecchi S, Wang Y, Delgado J, Casson Moreno V, Mignot M, Grénman H, et al. Bayesian  
517 Statistics to Elucidate the Kinetics of  $\gamma$ -Valerolactone from n-Butyl Levulinate Hydrogenation  
518 over Ru/C. *Ind Eng Chem Res* 2021;60:11725–36. <https://doi.org/10.1021/acs.iecr.1c02107>.
- 519 [54] Capecchi S, Wang Y, Casson Moreno V, Held C, Leveneur S. Solvent effect on the kinetics of  
520 the hydrogenation of n-butyl levulinate to  $\gamma$ -valerolactone. *Chem Eng Sci* 2021;231:116315.  
521 <https://doi.org/10.1016/j.ces.2020.116315>.
- 522 [55] Xu H, Hu D, Zhang M, Wang Y, Zhao Z, Jiang Z, et al. Bimetallic NiCu Alloy Catalysts for  
523 Hydrogenation of Levulinic Acid. *ACS Appl Nano Mater* 2021;4:3989–97.  
524 <https://doi.org/10.1021/acsanm.1c00339>.
- 525 [56] Al-Shaal MG, Wright WRH, Palkovits R. Exploring the ruthenium catalysed synthesis of  $\gamma$ -  
526 valerolactone in alcohols and utilisation of mild solvent-free reaction conditions. *Green Chem*  
527 2012;14:1260–3. <https://doi.org/10.1039/c2gc16631c>.
- 528 [57] Wang Y, Cipolletta M, Vernières-Hassimi L, Casson-Moreno V, Leveneur S. Application of  
529 the concept of Linear Free Energy Relationships to the hydrogenation of levulinic acid and its

- 530 corresponding esters. *Chem Eng J* 2019;374:822–31. <https://doi.org/10.1016/j.cej.2019.05.218>.
- 531 [58] Li C, Xu G, Zhai Y, Liu X, Ma Y, Zhang Y. Hydrogenation of biomass-derived ethyl  
532 levulinate into  $\Gamma$ -valerolactone by activated carbon supported bimetallic Ni and Fe catalysts.  
533 *Fuel* 2017;203:23–31. <https://doi.org/10.1016/j.fuel.2017.04.082>.
- 534 [59] Yan K, Chen A. Selective hydrogenation of furfural and levulinic acid to biofuels on the  
535 ecofriendly Cu–Fe catalyst. *Fuel* 2014;115:101–8.  
536 <https://doi.org/10.1016/J.FUEL.2013.06.042>.
- 537 [60] Li Z, Hao H, Lu J, Wu C, Gao R, Li J, et al. Role of the Cu-ZrO<sub>2</sub> interface in the  
538 hydrogenation of levulinic acid to  $\gamma$ -valerolactone. *J Energy Chem* 2021;61:446–58.  
539 <https://doi.org/10.1016/j.jechem.2021.01.046>.
- 540 [61] Fang S, Cui Z, Zhu Y, Wang C, Bai J, Zhang X, et al. In situ synthesis of biomass-derived  
541 Ni/C catalyst by self-reduction for the hydrogenation of levulinic acid to  $\Gamma$ -valerolactone. *J*  
542 *Energy Chem* 2019;37:204–14. <https://doi.org/10.1016/j.jechem.2019.03.021>.
- 543 [62] Orłowski I, Douthwaite M, Iqbal S, Hayward JS, Davies TE, Bartley JK, et al. The  
544 hydrogenation of levulinic acid to  $\Gamma$ -valerolactone over Cu–ZrO<sub>2</sub> catalysts prepared by a pH-  
545 gradient methodology. *J Energy Chem* 2019;36:15–24.  
546 <https://doi.org/10.1016/j.jechem.2019.01.015>.
- 547 [63] Shen Q, Zhang Y, Zhang Y, Tan S, Chen J. Transformations of biomass-based levulinate ester  
548 into  $\Gamma$ -valerolactone and pyrrolidones using carbon nanotubes-grafted N-heterocyclic carbene  
549 ruthenium complexes. *J Energy Chem* 2019;39:29–38.  
550 <https://doi.org/10.1016/j.jechem.2019.01.007>.
- 551 [64] Delgado J, Vasquez Salcedo WN, Bronzetti G, Casson Moreno V, Mignot M, Legros J, et al.  
552 Kinetic model assessment for the synthesis of  $\gamma$ -valerolactone from n-butyl levulinate and  
553 levulinic acid hydrogenation over the synergy effect of dual catalysts Ru/C and Amberlite IR-  
554 120. *Chem Eng J* 2022;430:133053. <https://doi.org/10.1016/j.cej.2021.133053>.

- 555 [65] Shimizu KI, Kanno S, Kon K. Hydrogenation of levulinic acid to  $\gamma$ -valerolactone by Ni and  
556 MoO<sub>x</sub> co-loaded carbon catalysts. *Green Chem* 2014;16:3899–903.  
557 <https://doi.org/10.1039/c4gc00735b>.
- 558 [66] Hengne AM, Malawadkar A V., Biradar NS, Rode C V. Surface synergism of an Ag-Ni/ZrO<sub>2</sub>  
559 nanocomposite for the catalytic transfer hydrogenation of bio-derived platform molecules. *RSC*  
560 *Adv* 2014;4:9730–6. <https://doi.org/10.1039/c3ra46495d>.
- 561 [67] Heeres H, Handana R, Chunai D, Borromeus Rasrendra C, Girisuta B, Jan Heeres H.  
562 Combined dehydration/(transfer)-hydrogenation of C<sub>6</sub>-sugars (D-glucose and D-fructose) to  $\gamma$ -  
563 valerolactone using ruthenium catalysts. *Green Chem* 2009;11:1247–55.  
564 <https://doi.org/10.1039/b904693c>.
- 565 [68] Fellay C, Dyson PJ, Laurency G. A viable hydrogen-storage system based on selective formic  
566 acid decomposition with a ruthenium catalyst. *Angew Chemie - Int Ed* 2008;47:3966–8.  
567 <https://doi.org/10.1002/anie.200800320>.
- 568 [69] Fábos V, Mika LT, Horváth IT. Selective conversion of levulinic and formic acids to  $\gamma$ -  
569 valerolactone with the shvo catalyst. *Organometallics* 2014;33:181–7.  
570 <https://doi.org/10.1021/om400938h>.
- 571 [70] Deng L, Zhao Y, Li J, Fu Y, Liao B, Guo QX. Conversion of levulinic acid and formic acid  
572 into  $\gamma$ -valerolactone over heterogeneous catalysts. *ChemSusChem* 2010;3:1172–5.  
573 <https://doi.org/10.1002/cssc.201000163>.
- 574 [71] Deng L, Li J, Lai DM, Fu Y, Guo QX. Catalytic conversion of biomass-derived carbohydrates  
575 into  $\gamma$ -valerolactone without using an external h<sub>2</sub> supply. *Angew Chemie - Int Ed*  
576 2009;48:6529–32. <https://doi.org/10.1002/anie.200902281>.
- 577 [72] Ruppert AM, Jędrzejczyk M, Sneka-Płatek O, Keller N, Dumon AS, Michel C, et al. Ru  
578 catalysts for levulinic acid hydrogenation with formic acid as a hydrogen source. *Green Chem*  
579 2016;18:2014–28. <https://doi.org/10.1039/c5gc02200b>.

- 580 [73] Yuan J, Li SS, Yu L, Liu YM, Cao Y, He HY, et al. Copper-based catalysts for the efficient  
581 conversion of carbohydrate biomass into  $\gamma$ -valerolactone in the absence of externally added  
582 hydrogen. *Energy Environ Sci* 2013;6:3308–13. <https://doi.org/10.1039/c3ee40857d>.
- 583 [74] Son PA, Nishimura S, Ebitani K. Production of  $\gamma$ -valerolactone from biomass-derived  
584 compounds using formic acid as a hydrogen source over supported metal catalysts in water  
585 solvent. *RSC Adv* 2014;4:10525–30. <https://doi.org/10.1039/c3ra47580h>.
- 586 [75] Li H, Fang Z, Yang S. Direct catalytic transformation of biomass derivatives into biofuel  
587 component  $\gamma$ -valerolactone with magnetic nickel-zirconium nanoparticles. *Chempluschem*  
588 2016;81:135–42. <https://doi.org/10.1002/cplu.201500492>.
- 589 [76] Chia M, Dumesic JA. Liquid-phase catalytic transfer hydrogenation and cyclization of  
590 levulinic acid and its esters to  $\gamma$ -valerolactone over metal oxide catalysts. *Chem Commun*  
591 2011;47:12233–5. <https://doi.org/10.1039/c1cc14748j>.
- 592 [77] Li H, Fang Z, Yang S. Direct Conversion of Sugars and Ethyl Levulinate into  $\gamma$ -Valerolactone  
593 with Superparamagnetic Acid-Base Bifunctional ZrFeOx Nanocatalysts. *ACS Sustain Chem*  
594 *Eng* 2016;4:236–46. <https://doi.org/10.1021/acssuschemeng.5b01480>.
- 595 [78] Ju Z, Feng S, Ren L, Lei T, Cheng H, Yu M, et al. Probing the mechanism of the conversion of  
596 methyl levulinate into  $\gamma$ -valerolactone catalyzed by Al(OiPr)<sub>3</sub> in an alcohol solvent: A DFT  
597 study. *RSC Adv* 2022;12:2788–97. <https://doi.org/10.1039/d1ra08429a>.
- 598 [79] Ortuño MA, Rellán-Piñeiro M, Luque R. Computational Mechanism of Methyl Levulinate  
599 Conversion to  $\gamma$ -Valerolactone on UiO-66 Metal Organic Frameworks. *ACS Sustain Chem Eng*  
600 2022;10:3567–73. <https://doi.org/10.1021/acssuschemeng.1c08021>.
- 601 [80] Chen X, Zhao T, Zhang X, Zhang Y, Yu H, Lyu Q, et al. Synthesis of ternary magnetic  
602 nanoparticles for enhanced catalytic conversion of biomass-derived methyl levulinate into  $\gamma$ -  
603 valerolactone. *J Energy Chem* 2021;63:430–41. <https://doi.org/10.1016/j.jechem.2021.07.013>.
- 604 [81] Zhang C, Huo Z, Ren D, Song Z, Liu Y, Jin F, et al. Catalytic transfer hydrogenation of



- 605 levulinate ester into  $\gamma$ -valerolactone over ternary Cu/ZnO/Al<sub>2</sub>O<sub>3</sub> catalyst. *J Energy Chem*  
606 2019;32:189–97. <https://doi.org/10.1016/j.jechem.2018.08.001>.
- 607 [82] Wu J, Zhu Y, Liao P, Xu T, Lu L, Zhang X, et al. Sustainable metal-lignosulfonate catalyst for  
608 efficient catalytic transfer hydrogenation of levulinic acid to  $\gamma$ -valerolactone. *Appl Catal A Gen*  
609 2022;635:118556. <https://doi.org/10.1016/j.apcata.2022.118556>.
- 610 [83] Protsenko II, Nikoshvili LZ, Matveeva VG, Sulman EM. Kinetic Modelling of Levulinic Acid  
611 Hydrogenation Over Ru-Containing Polymeric Catalyst. *Top Catal* 2020;63:243–53.  
612 <https://doi.org/10.1007/s11244-020-01223-0>.
- 613 [84] Huang X, Liu K, Vrijburg WL, Ouyang X, Iulian Dugulan A, Liu Y, et al. Hydrogenation of  
614 levulinic acid to  $\gamma$ -valerolactone over Fe-Re/TiO<sub>2</sub> catalysts. *Appl Catal B Environ*  
615 2020;278:119314. <https://doi.org/10.1016/j.apcatb.2020.119314>.
- 616 [85] Chalid M, Broekhuis AA, Heeres HJ. Experimental and kinetic modeling studies on the  
617 biphasic hydrogenation of levulinic acid to  $\gamma$ -valerolactone using a homogeneous water-soluble  
618 Ru-(TPPTS) catalyst. *J Mol Catal A Chem* 2011;341:14–21.  
619 <https://doi.org/10.1016/j.molcata.2011.04.004>.
- 620 [86] Abdelrahman OA, Heyden A, Bond JQ. Analysis of kinetics and reaction pathways in the  
621 aqueous-phase hydrogenation of levulinic acid to form  $\gamma$ -Valerolactone over Ru/C. *ACS Catal*  
622 2014;4:1171–81. <https://doi.org/10.1021/cs401177p>.
- 623 [87] Molleti J, Tiwari MS, Yadav GD. Novel synthesis of Ru/OMS catalyst by solvent-free method:  
624 Selective hydrogenation of levulinic acid to  $\Gamma$ -valerolactone in aqueous medium and kinetic  
625 modelling. *Chem Eng J* 2018;334:2488–99. <https://doi.org/10.1016/j.cej.2017.11.125>.
- 626 [88] Leveneur S, Pinchard M, Rimbault A, Safdari Shadloo M, Meyer T. Parameters affecting  
627 thermal risk through a kinetic model under adiabatic condition: Application to liquid-liquid  
628 reaction system. *Thermochim Acta* 2018;666:10–7. <https://doi.org/10.1016/j.tca.2018.05.024>.
- 629 [89] Cao CR, Liu SH. Thermal hazard characteristic evaluation of two low-temperature-reactive azo

- 630 compounds under adiabatic process conditions. *Process Saf Environ Prot* 2019;130:231–7.  
631 <https://doi.org/10.1016/j.psep.2019.08.020>.
- 632 [90] Bhattacharya A. A general kinetic model framework for the interpretation of adiabatic  
633 calorimeter rate data. *Chem Eng J* 2005;110:67–78. <https://doi.org/10.1016/j.cej.2005.05.003>.
- 634 [91] Stoessel F. *Thermal Safety of Chemical Processes: Risk Assessment and Process Design*.  
635 Wiley-VCH; 2008. <https://doi.org/10.1002/9783527621606>.
- 636 [92] Zheng JL, Wärnå J, Salmi T, Burel F, Taouk B, Leveneur S. Kinetic modeling strategy for an  
637 exothermic multiphase reactor system: Application to vegetable oils epoxidation using  
638 Prileschajew method. *AIChE J* 2016;62:726–41. <https://doi.org/10.1002/aic.15037>.
- 639 [93] Xie Q, Zhang Z, Zhang L, Xie Y, Liu W, Chen H. Thermal decomposition behavior and  
640 kinetics for nitrolysis solution from the nitration of hexamethylenetetramine. *React Kinet Mech*  
641 *Catal* 2019;128:645–62. <https://doi.org/10.1007/s11144-019-01658-x>.
- 642 [94] Andreozzi R, Canterino M, Caprio V, Di Somma I, Sanchirico R. Batch salicylic acid nitration  
643 by nitric acid/acetic acid mixture under isothermal, isoperibolic and adiabatic conditions. *J*  
644 *Hazard Mater* 2006;138:452–8. <https://doi.org/10.1016/j.jhazmat.2006.05.104>.
- 645 [95] Alamgir Ahmad K, Haider Siddiqui M, Pant KK, Nigam KDP, Shetti NP, Aminabhavi TM, et  
646 al. A critical review on suitability and catalytic production of butyl levulinate as a blending  
647 molecule for green diesel. *Chem Eng J* 2022;447:137550.  
648 <https://doi.org/10.1016/j.cej.2022.137550>.
- 649 [96] Delgado J, Vásquez Salcedo WN, Devouge-Boyer C, Hebert JP, Legros J, Renou B, et al.  
650 Reaction enthalpies for the hydrogenation of alkyl levulinates and levulinic acid on Ru/C–  
651 influence of experimental conditions and alkyl chain length. *Process Saf Environ Prot*  
652 2023;171:289–98. <https://doi.org/10.1016/j.psep.2023.01.025>.
- 653 [97] Zheng JL, Wärnå J, Salmi T, Burel F, Taouk B, Leveneur S. Kinetic modeling strategy for an  
654 exothermic multiphase reactor system: Application to vegetable oils epoxidation using

655 Prileschajew method. *AIChE J* 2016;62:726–41. <https://doi.org/10.1002/aic.15037>.

656 [98] Lavanchy F. Development of reaction calorimetry... - Google Scholar. n.d.

657 [99] Nasrifar K. Comparative study of eleven equations of state in predicting the thermodynamic  
658 properties of hydrogen. *Int J Hydrogen Energy* 2010;35:3802–11.  
659 <https://doi.org/10.1016/j.ijhydene.2010.01.032>.

660 [100] Stewart WE, Caracotsios M. *Computer-Aided Modeling of Reactive Systems*. First. New  
661 Jersey: 2008. <https://doi.org/10.1002/9780470282038>.

662 [101] Stewart WE, Caracotsios M, Sørensen JP. Parameter estimation from multiresponse data.  
663 *AIChE J* 1992. <https://doi.org/10.1002/aic.690380502>.

664 [102] Kopyscinski J, Choi J, Hill JM. Comprehensive kinetic study for pyridine  
665 hydrodenitrogenation on (Ni)WP/SiO<sub>2</sub> catalysts. *Appl Catal A Gen* 2012;445–446:50–60.  
666 <https://doi.org/10.1016/j.apcata.2012.08.027>.

667 [103] Van Boekel MAJS. Statistical aspects of kinetic modeling for food science problems. *J Food*  
668 *Sci* 1996;61:477–86. <https://doi.org/10.1111/j.1365-2621.1996.tb13138.x>.

669 [104] Caracotsios M, Stewart WE. Sensitivity analysis of initial value problems with mixed odes and  
670 algebraic equations. *Comput Chem Eng* 1985;9:359–65. [https://doi.org/10.1016/0098-](https://doi.org/10.1016/0098-1354(85)85014-6)  
671 [1354\(85\)85014-6](https://doi.org/10.1016/0098-1354(85)85014-6).

672 [105] Capecchi S, Wang Y, Delgado J, Casson Moreno V, Mignot M, Grénman H, et al. Bayesian  
673 Statistics to Elucidate the Kinetics of  $\gamma$ -Valerolactone from n-Butyl Levulinate Hydrogenation  
674 over Ru/C. *Ind Eng Chem Res* 2021;60:11725–36.  
675 [https://doi.org/10.1021/ACS.IECR.1C02107/ASSET/IMAGES/LARGE/IE1C02107\\_0008.JPEG](https://doi.org/10.1021/ACS.IECR.1C02107/ASSET/IMAGES/LARGE/IE1C02107_0008.JPEG)  
676 G.

677 [106] Ariba H, Wang Y, Devouge-Boyer C, Stateva RP, Leveneur S. Physicochemical Properties for  
678 the Reaction Systems: Levulinic Acid, Its Esters, and  $\gamma$ -Valerolactone. *J Chem Eng Data*  
679 2020;65:3008–20. <https://doi.org/10.1021/acs.jced.9b00965>.

680 [107] Lu X, Wang Y, Estel L, Kumar N, Grénman H, Leveneur S. Evolution of specific heat capacity  
681 with temperature for typical supports used for heterogeneous catalysts. *Processes* 2020;8:911.  
682 <https://doi.org/10.3390/PR8080911>.

683 [108] Toch K, Thybaut JW, Marin GB. A systematic methodology for kinetic modeling of chemical  
684 reactions applied to n-hexane hydroisomerization. *AIChE J* 2015;61:880–92.  
685 <https://doi.org/10.1002/aic.14680>.

686

687